Soil Dynamics and Earthquake Engineering 143 (2021) 106659

Contents lists available at ScienceDirect

Soil Dynamics and Earthquake Engineering

journal homepage: http://www.elsevier.com/locate/soildyn

Development of a hybrid control algorithm for effective reduction of drift in multispan isolated bridges

G. Heo [a], S. Seo [b], S. Jeon [b], C. Kim [a,*]

[a] Public Safety Research Center, Konyang University, 121 Daehangro, Nonsan, Chungcheongnam-do, 32992, South Korea
[b] Department of Civil Engineering and Informatics, Chungnam State University, 55 Haksa-gil, Cheongyang-gun, Chungcheongnam-do, 33303, South Korea

ARTICLE INFO

Keywords:
Structural drift control
Multispan isolated bridges
Control algorithm
MR damper

ABSTRACT

This study aimed to develop a hybrid control algorithm for semiactive control devices to effectively control the drift caused by seismic loads in the superstructure of an isolated multispan bridge. First, bridge behavior was simulated using the Newmark method to select a semiactive control device that would be appropriate for the bridge structure. An optimal control force was selected to control the displacement and relative displacement of each superstructure element. Next, an equation of motion that employed a stochastic linearization capable of representing the nonlinearity beyond the structural linear limits was used. Further, a Bouc–Wen model was designed to simulate the nonlinearity of the structure model and the control device to configure the control logic. A hybrid control algorithm was developed to overcome the disadvantages of the clipped-optimal and Lyapunov control algorithms, which show excellent control effectiveness but experience problems during nonlinear control along with extreme manual control problems owing to their use of the Heaviside step function. The two control algorithms were used individually to make judgments, and the results of each were used to produce a three-stage signal (min., max., median). The performance of the proposed control method with the developed algorithm was verified through experimental tests. The developed hybrid control algorithm improved the performance of the two individual control algorithms and effectively controlled the behavior of multispan bridges.

1. Introduction

Infrastructure facilities are threatened by various natural disasters. In particular, bridges are at risk of damage and even collapse. These risks arise owing to pounding in the superstructure or large external forces such as seismic loads, especially if these issues are not considered during design. Currently, advanced construction technologies are enabling the construction of more stable bridges. Nonetheless, old-fashioned multispan bridges consisting of two superstructures arranged in series and centered on piers remain in wide use even today. Most such bridges are made of concrete (or reinforced concrete), and expansion joints are placed in the connecting parts of the superstructure to minimize damage due to temperature changes. The intervals between the superstructure sections created by these expansion joints are a source of pounding between adjacent elements; such pounding is usually caused by the longitudinal drift occurring in the superstructure owing to the effect of external loads such as earthquakes. Pounding due to the drift of bridge superstructures was observed during the 1989 Lome Prita earthquake, 1994 Northridge earthquake, and 2001 Bhuj earthquake [1–3]. By contrast, large-scale pounding did not occur in the superstructure elements during the 2017 Pohang earthquake and the 2011 Great East Japan earthquake; superstructure drift only resulted in some deformation and damage of the isolation devices [4,5].

Bridges are important pathways for response and recovery operations when earthquakes occur. If a bridge superstructure suffers drift because of seismic loads, access to the bridge may be limited, thereby hampering these operations. Domaneschi and Martinelli discussed the resilience of seismic control solutions for bridges through case studies and confirmed that the application of control devices had positive effects on structural restoration [6]. Other studies have investigated the use of various control devices to reduce drift in bridge superstructures, such as steel restrainers, metallic dampers, viscoelastic (VE) dampers, and magnetorheological (MR) dampers [7–11]. Among these devices, MR dampers are often used as semiactive control devices for controlling bridge vibrations by regulating the current input [12–14]. Ruangrassamee and Kawashima, Guo et al., and Sheikh et al. conducted representative experimental and analytical studies of the control of bridge vibrations, specifically, the control of bridge pounding, through

* Corresponding author.
E-mail addresses: heo@konyang.ac.kr (G. Heo), seo@cnsu.ac.kr (S. Seo), Jeon@cnsu.ac.kr (S. Jeon), cg-kim@konyang.ac.kr, cg-kim@hanmail.net (C. Kim).

https://doi.org/10.1016/j.soildyn.2021.106659
Received 24 March 2020; Received in revised form 24 June 2020; Accepted 8 January 2021
Available online 20 February 2021

the use of MR dampers [9,15,16]. Guo et al. studied three types of MR damper performance, namely passive-off, passive-on, and semiactive control [15]. Sheikh et al. applied a bang–bang control algorithm to semiactive control [16].

The advantages of MR dampers are that they allow for smoother control than a friction-type damping device does, and their control force can be adjusted according to the control signals. However, they are disadvantageous because they require an external power source, and it is important to carefully select a control algorithm as it strongly influences their performance. Therefore, some studies investigated various control algorithms to obtain the optimal MR damper performance. Heo et al. experimentally evaluated a control algorithm based on the Lyapunov direct method and another based on the clipped-optimal control algorithm to control vibrations in adjacent bridge decks via a semiactive control device [17]. Both algorithms are often applied to MR dampers for vibration control, and their performance has been evaluated in various studies. Both algorithms are effective in linear systems but not in nonlinear one, such as the nonlinear behavior of isolated devices occurring owing to seismic loads. Further, these algorithms use overly conservative parameters that can induce an excessive system response [18,19]. Finally, these algorithms cannot easily control nonlinear behaviors when the voltage input is limited to simply 0 or 1 [18,20]. Therefore, a more improved algorithm must be developed for controlling nonlinear behaviors.

In this light, the present study proposes a control method in which a semiactive control device is used to protect multispan bridges from damage and collapse by effectively controlling the longitudinal drift caused by pounding between adjacent superstructure elements during earthquakes. This method is verified analytically and experimentally. This study also develops a hybrid control algorithm that can overcome the disadvantages of the Lyapunov and the clipped-optimal control algorithms that are often used for drift control. To verify the validity of the proposed control method with the developed hybrid control algorithm, shaking table tests were performed on a multispan isolated bridge model. Finally, the differences between this hybrid control algorithm and existing control algorithms were examined; the hybrid control algorithm was confirmed to effectively control drift in multispan isolated bridges.

2. Multispan bridge drift control methods and assumptions

2.1. Multispan isolated bridge drift control methods

Generally, a bridge consists of a deck that is a part of its superstructure, piers, abutments that support the deck, and isolation equipment that is installed to prevent the substructure's vibrations from being transferred to the superstructure. However, even in bridges with installed isolation equipment, pounding can occur between superstructure elements owing to the effects of nonuniform ground motion. Therefore, additional dampers are used to prevent pounding and collapse due to vibrations in the superstructure. Dampers, one such additionally installed control device, are used to support the piers and abutments to control the movement of the superstructure. Dampers, when configured suitably, can successfully control the vibrations in the superstructure when large forces such as earthquakes act on the bridge. However, damage may occur when an additional force that has not been reflected in the design acts on the piers and abutments.

Previous studies developed and experimentally evaluated the performance of a drift control method that would not have an additional effect on the piers while connecting the spans by a semiactive control device to use the behavior energy of adjacent superstructure elements in the structure's overall drift control [17]. The control logic of the proposed method considered the control device's nonlinearity but not the target structure's nonlinearity. This study extends previously proposed methods and presents a multispan isolated bridge control method that accounts for the nonlinearity of the structure.

Fig. 1 shows a multispan bridge drift control method. Here, x is the displacement relative to the ground displacement of each superstructure component; $\ddot{x}_g$ is the ground acceleration; m, c, and k are the bridge's mass, damping, and stiffness, respectively; z is the hysteresis factor; and F_{MR} is the semiactive control device's control force. Normal linearization, which is the basis of the motion equations used to control structures, is used to complete the system based on a linear stiffness that depends on the initial stiffness of each structural element. Because this type of linearization ignores the structure's nonlinearity, an inaccurate response may be produced when drift occurs owing to a load that exceeds the material's limit. To overcome the limitations of this type of linearization, the proposed control method includes a structure model that is based on stochastic linearization. Stochastic linearization expresses the nonlinear history elements as equivalent time-invariant models by minimizing the error that occurs in the linearization process [21]. The motion equation that uses a stochastic linearization strategy for the multispan bridge system shown in Fig. 1 is as follows:

$$\mathbf{M}\ddot{\mathbf{U}} + \mathbf{C_d}\dot{\mathbf{U}} + \mathbf{K_u}\mathbf{U} + \mathbf{K_z}\mathbf{Z} = -\mathbf{M}\ddot{x}_g \tag{1}$$

Here, $\mathbf{M}$ and $\mathbf{C_d}$ are the mass and damping, respectively; $\mathbf{K_u}$ and $\mathbf{K_z}$ are the linear and the nonlinear stiffness matrix, respectively; and $\mathbf{U}$, $\mathbf{Z}$ and $\ddot{x}_g$ are the displacement vector ($[x_1,\ x_2,\ x_3]$), hysteresis element vector, and ground acceleration in Fig. 1, respectively. The $\mathbf{Z}$ matrix includes the hysteresis element ($[z_1,\ z_2,\ z_3]$) marked in Fig. 1 and the history element of the semiactive control device ($[z_4,\ z_5]$). The hysteresis element z is an evolutionary variable defined by the Bouc–Wen differential equation shown in Eq. (2).

$$\dot{z} = A_i\dot{x}_i - \beta_i\left|\dot{x}_i\right|z_i - \gamma_i\dot{x}_i|z_i| \tag{2}$$

Here, the subscripts $i(=1,\cdots,5)$ represent three spans (A, B, and C) and two dampers (F_{MR1} and F_{MR2}), respectively. $\dot{x}$ is the velocity, and A, β, and γ are parameters that control the shape of the loop. Eq. (2) depends only on the velocity and hysteresis; therefore, it can be expressed using the following equivalent linearization equation:

$$\dot{z}_i = -C_i\dot{x}_i - K_i z_i \tag{3}$$

Here, C_i and K_i are linearized parameters of velocity and hysteresis terms, respectively. To linearize the nonlinear elements that are included in the motion equation by using the stochastic linearization strategy of Eq. (1), the multispan isolated bridge's superstructure and the Bouc–Wen model (semiactive control device model) were used, and then, the convergence process was performed to complete the linearized bridge model in Eq. (4) [22,23].

$$\dot{\mathbf{X}} = \mathbf{A_{state}}\mathbf{X} + \mathbf{F_e} \tag{4}$$

Here, $\mathbf{X}$ is a state vector that consists of $[\mathbf{U};\ \dot{\mathbf{U}};\ \mathbf{Z}]$, $\mathbf{F_e}(=[0\ \ -\ddot{x}_g\ 0]')$ is an external force vector by $\ddot{x}_g$, and $\mathbf{A_{state}}$ is the system matrix as expressed in Eq. (5).

$$\mathbf{A_{state}} = \begin{bmatrix} 0 & \mathbf{I} & 0 \\ -\mathbf{M}^{-1}\mathbf{K_u} & -\mathbf{M}^{-1}\mathbf{C_d} & -\mathbf{M}^{-1}\mathbf{K_z} \\ 0 & \mathbf{C_b} & \mathbf{K_b} \end{bmatrix} \tag{5}$$

Here, $\mathbf{C_b}$ and $\mathbf{K_b}$ are linearized parameters for the system's speed and history elements, respectively. These parameters are repeatedly adjusted until the displacement responses obtained from experiments performed on the real structure correspond to the simulated ones for the whole three-span bridge structure by inputting the initial values acquired from the dampers.

2.2. Assumptions of drift control for a multispan bridge

The major factors influencing the pounding of a bridge superstructure caused by external loads such as earthquakes are the differences in the dynamic characteristics of adjacent structures and the

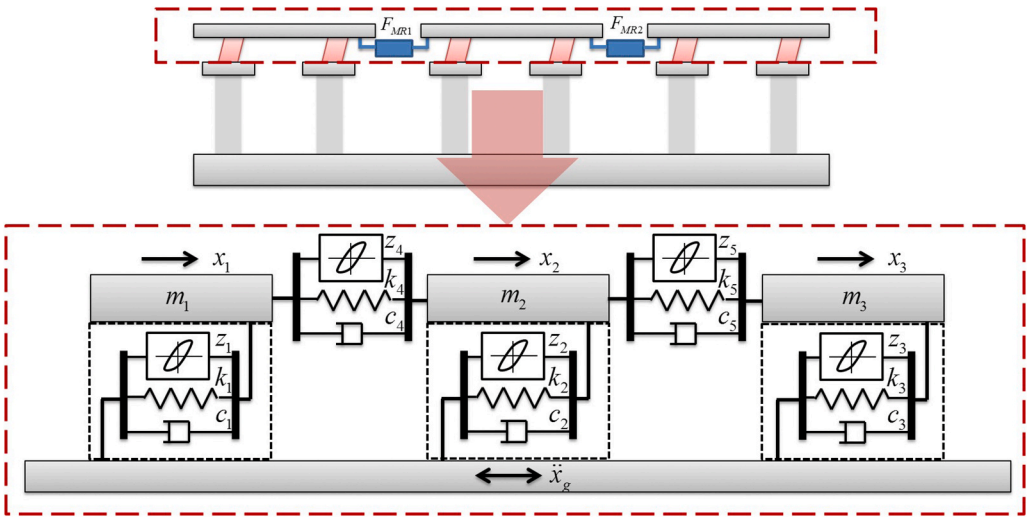

Fig. 1. Connecting multispan bridge's control devices.

multidimensional behavior of the ground. Among those factors, this study focused on the differences in the dynamic characteristics of adjacent structures. Therefore, the ground movement was assumed to be transferred along the longitudinal direction of the bridge. This study did not consider the up and down impacts to the bridge's superstructure and substructure, which includes the piers and abutments that support the superstructure; the lateral external forces that act on the bridge; and the bridge's lateral behavior.

As mentioned before, an isolated bridge with isolated devices comprises a substructure that includes the piers and foundations and a superstructure that includes the deck of the bridge. Isolation devices are installed between the superstructure and the substructure to isolate the transfer of vibrations between them and to support the superstructure. The mass affects the behavior of the bridge and is mainly concentrated in the superstructure. The stiffness of the isolation device is very small than that of the substructure; therefore, the response of the bridge can be assumed to be determined by the behavior of the superstructure.

In this study, these assumptions were used to create a multispan bridge model that has three continuous superstructure spans, as shown in Fig. 2.

As shown in Fig. 2(a), the multispan isolated bridge model is a continuous bridge with three spans that are longitudinally continuous, and abutments are installed at the left and right ends of the bridge. Span B, which is 2.5 times larger than spans A and C, was installed to examine the pounding between adjacent superstructure components that can occur owing to differences in the dynamic characteristics of the adjacent structures. As shown in Fig. 2(b), the bridge superstructure has two girders (longitudinal I-beams) placed below 100 *mm* thick reinforced concrete slabs; these beams resist bending in the slabs. A cross beam was placed between the longitudinal I-beams to prevent the deformation of

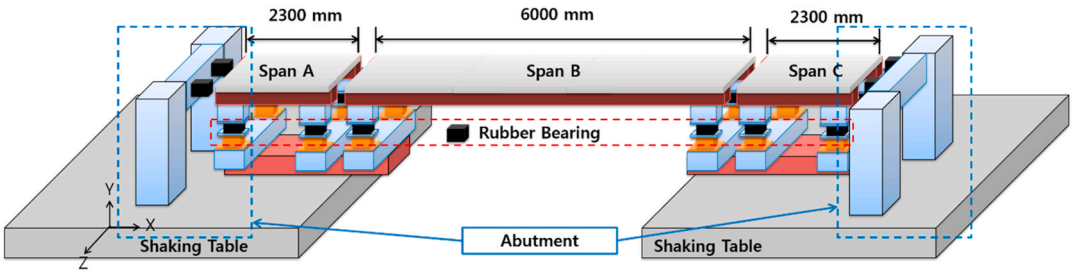

(a) Multispan isolated bridge model

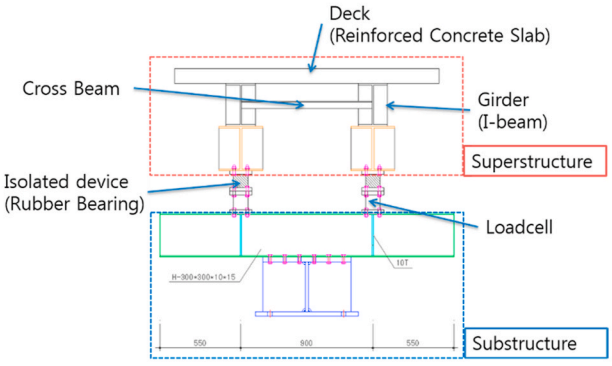

(b) Construction of model bridge

Fig. 2. Model bridge for multispan bridge drift control.

the superstructure. This superstructure was placed above an isolation device (rubber bearing), and a load cell was used to measure the control force of the isolation device. Each span was supported by four rubber bearings to resist a total shear strength of 240 kN/m. The substructure was designed to only the support the superstructure. In the multispan bridge shown in Fig. 2, spans A and C have a length of 2.3 m and span B has a length of 6 m. The weights of the spans including the jigs for installing the MR dampers are 1490, 3520, and 1520 kg for spans A, B, and C, respectively. Each span is supported by four rubber bearings. As assumed previously, the response of the bridge is determined by the bridge superstructure elements (spans). Therefore, the piers of the substructure were simply built to support the superstructure. Structures that simulate abutments were installed at the left and right ends of the multispan isolated bridge, and the abutment impacts of spans A and C were considered.

3. Relationship between semiactive control device and control algorithm

3.1. Calculating optimal control force

This study proposes a control method that connects adjacent superstructure elements through semiactive control devices to prevent pounding and to control the vibrations in a multispan isolated bridge. This control method does not apply an additional external force to the piers or abutments. However, when the control force of the control device is stronger than the behavior energy of the superstructure due to the external force, the multiple superstructures connected to the control device may together exhibit the same large movement as one structure. This type of unified drift can prevent pounding between adjacent superstructure elements; however, it serves to increase the bridge's overall behavior. Therefore, this study calculated the optimal control force required for the effective control of the bridge before selecting the semiactive control device. Here, the optimum control force refers to the maximum control force in a state where no harmful behavior occurs owing to the application of the control device. To calculate the optimal control force, this study used a normal Newmark method function (a multiple-degree-of-freedom (MDOF) system time integration) that utilizes an adaptive control-style structural simulation. A normal algorithm for structural dynamics was used. The seismic loads of the Kobe seismic waves (measured by the KJMA observatory station in 1995), which are typical of near-field seismic loads, and the El Centro seismic waves (measured as PGA 0.313 g at the 117 El Centro Array #9 in 1940), which are typical of far-field seismic loads, were used as the external forces for the simulation. The structure for the simulation was programmed based on the equation of motion (Eq. (1)), and the masses of spans A and B were used as the actual measured values described in Section 2.2. Because the mass of span C is only slightly different from that of span A, the same value as that of span A was used. The semiactive control device model and the structure stiffness model were applied to the 30 kN MR damper Bingham plastic model and the rubber-bearing Bouc–Wen model proposed by Heo et al. [24]. As shown in Fig. 2(a), in the multispan bridge model, the two spans (A and C) located around span B in the center have the same mass and stiffness. Therefore, the simulation was performed under the assumption that spans A and C show the same behavior when an external force is applied. Here, because the rigidity of the structure depends on the characteristics of the base isolation device below the superstructure, only the behavior of the base isolation device was considered. The simulation was divided into a basic structure state in which the control device was not installed, a state in which adjacent superstructure elements were connected by the control device and four currents (0, 1, 2, and 3 A) were supplied, and a rigid state in which adjacent superstructure elements were connected by rigid bodies. The simulation confirmed that the drift of each span was caused by the input seismic loads. Matlab code was used to operate the simulation program, and Table 1 lists the calculated simulation results.

Table 1
Simulation results of Kobe earthquake.

Estimation Results Control Case	Displacement (mm)				Force (N)
	Each Span			Relative	
	Span A	Span B	Span C	A–B & B–C	A–B & B–C
BARE	7.7974	37.458	7.7974	38.3326	0
0A	12.385	15.811	12.385	11.1409	4824.1938
1A	20.28	20.411	20.28	0.85678	9911.0885
2A	20.526	20.571	20.28	0.41029	10277.377
3A	20.594	20.628	20.594	0.32049	10314.194
RIGID	20.619	20.649	20.619	0.28743	10350.765

As observed in Tables 1 and 2, when the 30 kN MR damper was used to perform multispan bridge drift control, the relative displacement was reduced by more than 70% in the 0 A state, that is, when current was not supplied, compared with the basic structure state (BARE). When a current of 1 A or more was supplied, it was predicted that the three independent bridges would show unified behavior similar to that in the rigid state. Therefore, the 30 kN MR damper was found to be unsuitable when confirming the performance using the control algorithm for the semiactive control device for multispan bridge control.

Because of these simulation results, an additional simulation was performed to find the optimal control force that is suitable for drift control in this study's target multispan isolated bridge model. In this additional simulation, the damping value of the MR damper was increased and the structure's behavior was examined. The graph in Fig. 3 shows the changes in displacement that occurred under each simulation condition.

In the simulation, the damping value of the MR damper increased from 0 to 35 ton/s in 5 ton/s intervals. In the acquired data, the relative displacement between spans A and B was observed. The graph in Fig. 3 (a) shows the trend of decrease (amount of decrease in current stage compared with all stages) in the relative displacement for each condition (damping value) as the damping value of the MR damper was increased. This graph shows that the use of a damping value resulted in the relative displacement decreasing by 12 mm compared with that when the damping value was 0. However, as the damping value increased, the relative displacement decreased by a smaller amount than that under the previous condition. For a damping value of 10 ton/s or more, the decrease was less than 5 mm, and at 30 ton/s or more, the decrease was less than 1 mm. In other words, when a damping value of 30 ton/s or more was used, the relative displacement between spans A and B was predicted to show a unified behavior in which no further reduction occurred. The graphs in Fig. 3 (b)–(d) show the simulation results in which the MR damper's damping value was increased in 1 ton/s intervals from 0 to 12 ton/s to observe the changes in the structure's behavior at damping values below 10 ton/s. Graph (b) shows the trend of decrease in the relative displacement between spans A and B. This graph shows that when a damping value of 7 ton/s or more was used, the relative displacement decreased by a markedly smaller amount than that under the previous condition (damping value: 6 ton/s). Graph (d) shows a similar trend for the decrease in the displacement of span B at each

Table 2
Simulation results of El Centro earthquake.

Estimation Results Control Case	Displacement (mm)				Force (N)
	Each Span			Relative	
	Span A	Span B	Span C	A–B & B–C	A–B & B–C
BARE	10.5888	59.2687	10.5888	64.5471	0
0A	12.9997	13.996	12.9997	8.6434	5148.9289
1A	15.7595	15.8538	15.7595	0.56273	7888.3863
2A	15.942	15.9982	15.942	0.32545	7988.7637
3A	15.9979	16.042	15.9979	0.25444	8019.3153
RIGID	16.0187	16.0582	16.0187	0.22829	8030.627

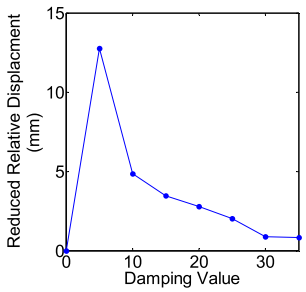

(a) Changes in relative displacement reduction with 5 ton/s increase intervals in damping value

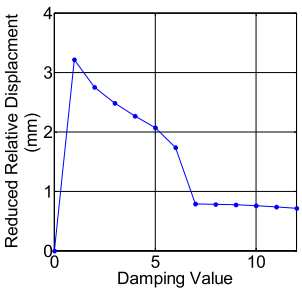

(b) Changes in relative displacement reduction with 1 ton/s increase intervals in damping value

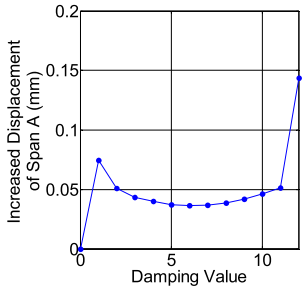

(c) Changes in increased displacement of span A according to damping value

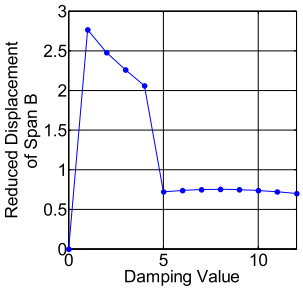

(d) Changes in increased displacement of span B according to damping value

Fig. 3. Simulation results obtained with different damping values.

stage. Graph (c) shows the behavior changes in span (A) under each condition. In span A, the amount of increase in displacement compared with that in the previous condition began to decrease as the damping value of the MR damper increased. However, for a damping value of 6 ton/s or more, the amount of increase in displacement began to increase again. From these simulation results, it is predicted that setting the MR damper's damping value at 6 ton/s or more may positively affect the relative displacement between spans A and B and the reduction in displacement of span B; however, a problem occurs at the value where span A's displacement increases again. The optimal control force of the MR damper was found to be that when a damping value of 6 ton/s was used.

Table 3 lists the simulation results in which the MR damper's damping value was increased in 1 ton/s intervals from 0 to 12 ton/s. This table shows that the MR damper's maximum control force was 2.164 Nat a damping value of 6 ton/s.

3.2. Semiactive control device

To perform appropriate control according to the current state of the bridge, a control device that can adjust the control force is needed. For the control device, this study selected an MR damper that can adjust the control force according to external control signals (current) to control the vibrations in a multispan bridge. For the MR damper, this study selected the cylinder-type RD-8040-1 model (LORD) with an allowed stroke displacement of ± 27.5 mm and a maximum control force of 2 kN that can match the optimal control force calculation results. Its advantage is that the control force can be adjusted easily by varying the current; however, its disadvantage is that it is vulnerable to the effects of the temperature caused by the application of the current. To develop the selected MR damper model, its dynamic characteristics were experimentally tested using a spring testing device. The tests were performed at a maximum displacement of ± 10 mm, 1 Hz, and 0.0628 m/s under four conditions according to the supplied current (0, 0.5, 1, and 1.5 A). Further, the MR damper can intermittently provide current at 2 A, and additional tests were performed at a current of 2 A. During the tests, stable current was supplied to the damper using a PMC 18-3A. The tests measured the damper's control force data and stroke displacement. The control force is the output value of the load cell (DBBP-2t). The displacement is the output value of the sensor installed in the testing device itself. Fig. 4 shows a force–displacement graph and a force–speed graph according to the changes in the current supplied to the MR damper. This graph shows that the control force increased according to the current supplied to the MR damper selected in this study. However, at a current of 1.0 A or more, the range of increase in the control force was reduced.

Table 3
Simulation results according to damping values used (El Centro).

Estimation Results Damping Value	Displacement (mm)				Force (N)
	Each Span			Relative	
	Span A	Span B	Span C	A–B & B–C	A–B & B–C
0	7.7974	37.4580	7.7974	38.3326	0
1	7.8719	34.6969	7.8719	35.1221	466.57
2	7.9227	32.2221	7.9227	32.3753	835.63
3	7.9662	29.9649	7.9662	29.8919	1203.9
4	8.0061	27.9094	8.0061	27.6293	1577.3
5	8.0434	27.1870	8.0434	25.5610	1876.7
6	**8.0797**	**26.4481**	**8.0797**	**23.8221**	**2164.1**
7	8.1163	25.6991	8.1163	23.0351	2422.8
8	8.1550	24.9471	8.1550	22.2530	2656.5
9	8.1970	24.1998	8.1970	21.4809	2868.7
10	8.2433	23.4635	8.2433	20.7235	3062.3

A control device model that used the control algorithm was developed based on the data acquired from the performance test results of the MR damper. The MR damper model was developed using the Bouc–Wen model; Tables 4 and 5 list the parameters of the developed model.

Each parameter in Tables 4 and 5 was determined using a global optimization method based on gradient descent, which minimizes the error cost function between the experimental and simulation results. Finally, the control force (F_{MR}) of the MR damper is calculated as

$$F_{MR} = \alpha_{\dot{x}_{MR}}\dot{x} + \alpha_{z_{MR}}z \tag{6}$$

Here, $\dot{x}$ is the velocity of the hysteresis component; z is the

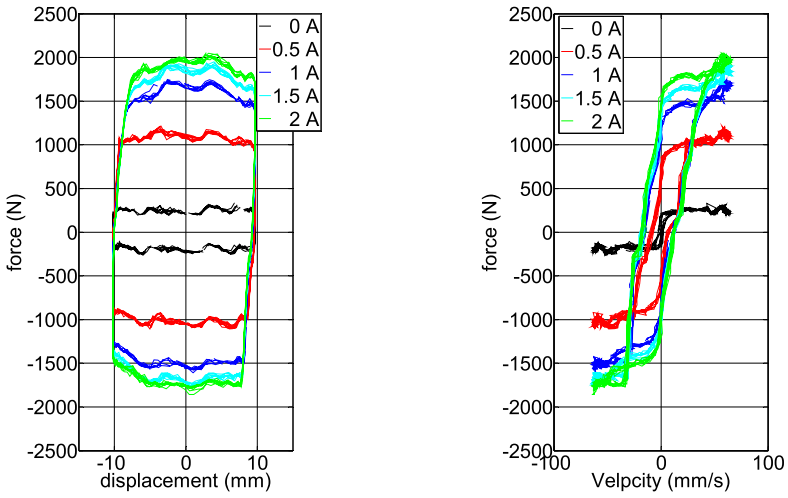

(a) Force–displacement response according to current supply

(b) Force–velocity response according to current supply

Fig. 4. MR damper performance test results.

Table 4
Parameters that control the shape of the loop.

A_{MR}	β_{MR}	γ_{MR}
45.48	0.56	1.38

Table 5
Bouc–Wen model parameters.

$\alpha_{\dot{x}_{MR0}}$	$\alpha_{z_{MR0}}$
14 $N{\cdot}sec/mm$	7.0 N/mm
$\alpha_{\dot{x}_{MR1}}$	$\alpha_{z_{MR1}}$
13.1 $N{\cdot}\ sec/\ mm.Amp$	51.9 $N/mm.Amp$
$\alpha_{\dot{x}_{MR2}}$	$\alpha_{z_{MR2}}$
$-5.7\ N{\cdot}\ sec/\ mm.\ Amp^2$	$-10.3\ N/mm.Amp^2$

evolutionary variable defined by Eq. (2); and $\alpha_{\dot{x}_{MR}}$ and $\alpha_{z_{MR}}$ are respectively the damping and hysteresis components of MR dampers and are calculated by applying the Bouc–Wen model parameters in Table 5 to the input current function given by the following equation:

$$\begin{aligned}\alpha_{\dot{x}_{MR}} &= \alpha_{\dot{x}_{MR0}} + i_c\alpha_{\dot{x}_{MR1}} + i_c^2\alpha_{\dot{x}_{MR2}}\\ \alpha_{z_{MR}} &= \alpha_{z_{MR0}} + i_c\alpha_{z_{MR1}} + i_c^2\alpha_{z_{MR2}}\end{aligned} \tag{7}$$

Here, i_c is the input current supplied to the MR damper. In this study, input currents of 0, 1, and 2 A were used. Table 5 and Fig. 5 show the experimental and simulation results when a current of 1 A is supplied to the MR damper.

Fig. 5(a) and (b) respectively show the force–displacement and force–velocity responses, which are consistent with the results of the Bouc–Wen model.

3.3. Control algorithm

To perform drift control effectively, it is necessary to provide a control device and a control algorithm based on the required control condition of the bridge. To develop a new effective hybrid control algorithm, the Lyapunov stability-based control algorithm and the clipped-optimal control algorithm [25,26] are adopted; previous studies have confirmed these to be effective. The control effectiveness of both algorithms was examined to develop a control strategy that combines the two.

The Lyapunov stability-based control algorithm is a control strategy that adjusts the control force using Eq. (8), ensuring that the behavior of the structure to be controlled is within a fixed distance from a stability point.

$$v_{i_{Ly}} = V_{max}H\left(\left(-z^T\right)PB_if_i\right) \tag{8}$$

Here, V_{max} is the maximum voltage that can be supplied to the control device; H, the Heaviside step function; $v_{i_{Ly}}$, the control voltage supplied to the control device; f_i, the current control force of the i^{th} control device; P, the positive definite matrix; B, the position matrix of the control device; and z, the hysteresis element derived from Eq. (4). The current control force is measured using a load cell attached to each damper. Eq. (8) is determined by the derivation of the Lyapunov function in Eq. (9).

$$V(z) = \frac{1}{2}z_p^2 \tag{9}$$

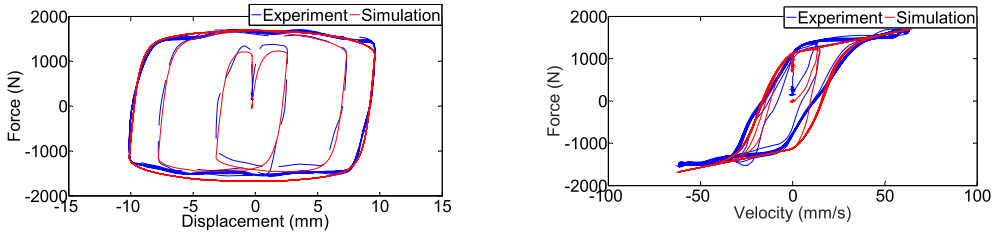

(a) Force–displacement response

(b) Force–velocity response

Fig. 5. Comparison of MR damper model and performance test results.

If Eq. (9) is derived, ultimately, only $z^T PBf$ remains as an adjustable term that can produce the control effect. Here, z_p is the P-norm defined in Eq. (10).

$$z_p = \left[z^T P z\right]^{1/2} \tag{10}$$

The clipped-optimal control algorithm controls the vibration by adjusting the controller's control force so that it satisfies the calculated required control force (f_c). Specifically, the voltage supplied to the control device is adjusted according to Eq. (11) so that the control force created by the current control device satisfies the calculated control force that is required for the bridge using the designed linear optimal controller ($K_c(s)$).

$$v_{i_{Cl}} = V_{max} H(\{f_{ci} - f_i\} f_i) \tag{11}$$

Here, V_{max} is the maximum voltage that can be supplied to the control device; H, the Heaviside step function; $v_{i_{Cl}}$, the control voltage supplied to the control device; and f_{ci}, the i^{th} control device's required control force. The control force required to control the vibration of the bridge is calculated as

$$f_{ci} = L^{-1}\left\{ -K_c(s) L\left\{ \begin{matrix} y \\ f_i \end{matrix} \right\} \right\} \tag{12}$$

Here, $L(\cdot)$is the Laplace transform operator and y, the structure's measured response.

3.4. Hybrid control algorithm

As discussed in the introduction, both the Lyapunov and the clipped-optimal control algorithms clearly work well in the linear system. However, when some random load is applied, as in an earthquake, vibration isolation devices behave in a nonlinear manner. In particular, when a bridge superstructure comprises multiple spans connected by MR dampers to control bridge vibrations, it can structurally behave in a nonlinear manner. Therefore, to apply the Lyapunov and clipped-optimal control algorithms, nonlinear behaviors were linearized by a stochastic linearization strategy (see 2.1 and Eqs. (1)–(4)). However, these two control algorithms have only a limited capacity for controlling multispan bridges owing to their control features and specific approaches; in particular, the clipped-optimal control algorithm tends to stabilize forces whereas the Lyapunov algorithm tends to stabilize the system itself. Specifically, because the signals are limited to only 0 (off) and 1 (on), they are inherently limited for the control of structural nonlinear behaviors. Therefore, we developed a hybrid control algorithm specially for nonlinear behaviors after linearizing them. It combines the system-stabilization capability of the Lyapunov control algorithm with the force-stabilization capability of the clipped-optimal control algorithm; at the same time, it enables the control device to calculate a median value in the case where these two algorithms contradict each other during control.

$$v_{i_{Comp}} = \begin{cases} 0, \ if \ v_{i_{Ly}} + v_{i_{Cl}} = 0 \\ 0.5, \ if \ v_{i_{Ly}} + v_{i_{Cl}} = 1 \\ 1, \ if \ v_{i_{Ly}} + v_{i_{Cl}} = 2 \end{cases} \tag{13}$$

Here, $v_{i_{Comp}}$ is the hybrid control voltage that is produced according to the relational conditions, and $v_{i_{Ly}}$ and $v_{i_{Cl}}$ are the control voltages that are calculated by the Lyapunov control algorithm and the clipped-optimal control algorithm, respectively. In the control algorithm given by Eqs. (13) and (0) is produced as the calculation result of the two algorithms if both algorithms determine that control is not needed, 0.5 is produced if only one of the two algorithms determines that control is needed, and 1 is produced if both algorithms determine that control is needed. In other words, a 0.5 intermediate control signal is added to the control signals, which were limited to 0 and 1. This step minimizes the excessive response errors that can occur in one of the two algorithms. When the two algorithms have matching opinions, they are 100% reliable, and a signal of 0 or 1 is produced.

Fig. 6(a) shows the flow of the developed control algorithm. First, the structure response (x, $\ddot{x}$) and current control forces (f_i) due to external forces are measured. Next, the clipped-optimal control algorithm and the Lyapunov control algorithm are operated on the basis of the structure response and the current control forces, and the judgment result of each algorithm is obtained as the output. Here, the required control force of the clipped-optimal control algorithm and the hysteresis element vector of the Lyapunov control algorithm are obtained through the linear optimal controller and observer by using Eq. (1) based on stochastic linearization, respectively Finally, the current for controlling the MR damper is output in accordance with the control condition of the hybrid control algorithm given by Eq. (13). To experimentally evaluate the control performance, the developed control algorithm is programmed with Matlab and Simulink as shown in Fig. 6(b).

In Fig. 6(b), the left yellow block is the response measured from the structure; the gray block is the linear optimal controller and the observer; the green block is the clipped-optimal control algorithm; and the cyan block is the Lyapunov control algorithm.

4. Real-time drift control test

4.1. Configuration of real-time drift control system

To experimentally evaluate the performance of the hybrid control algorithm that was developed to reduce drift in multispan isolated bridges, the multispan isolated bridge model shown in Fig. 2 was built as shown in Fig. 7.

Fig. 7(a) shows the multispan bridge behavior caused by an external force in the situation where the control device is not being used. As shown in this figure, span B is the middle part and has a relatively large mass, and it collides with spans A and C owing to the large drift caused by the external force. Fig. 7(b) shows the bridge behavior caused by the external force in the situation where two adjacent spans are connected by a control device. When the control device is being used, if sufficient control is achieved, a separation distance is maintained between the three spans and they do not collide with each other. Accordingly, the selected MR dampers were used between two adjacent spans, as shown in Fig. 7(c).

To effectively control vibrations in a structure by using the MR damper semiactive control device, it is necessary to have a measurement system that can capture the current state of the structure, an intermediate processing device that can analyze the measured data and determine whether or not control is applied, and a control system that controls the MR dampers based on the signal produced depending on whether or not control is applied. This study used a dSPACE CP1103 measurement and control system for the input of signals measured from the structure and the output of signals sent to the control system. The special-use program Control Desk was used to run dSPACE CP1103, and the Matlab and Simulink programs were used to implement the measurement and control logic. To measure the structure's response to an external force, this study used a Dytran 3134D accelerometer and a KTR-B-100 *mm* displacement sensor (Minor Tech). To measure the current control force of the MR damper, a DBBP-2t load cell (Bongshin) was used. To control the MR damper, a PMC 18-3A DC power supply (KIKUSUI) was used. Tables 6 and 7 show details of the software and hardware used in the tests, respectively.

4.2. Real-time drift control test conditions

To evaluate the performance of the hybrid algorithm that was developed to effectively reduce drift in multispan isolated bridges, two shaking tables (MST) from Korea's Seismic Simulation Test Center were used. Preparatory tests were performed to confirm that the shaking tables were synchronized before performing the real-time drift control tests. Fig. 8 shows a graph that compares the data measured after

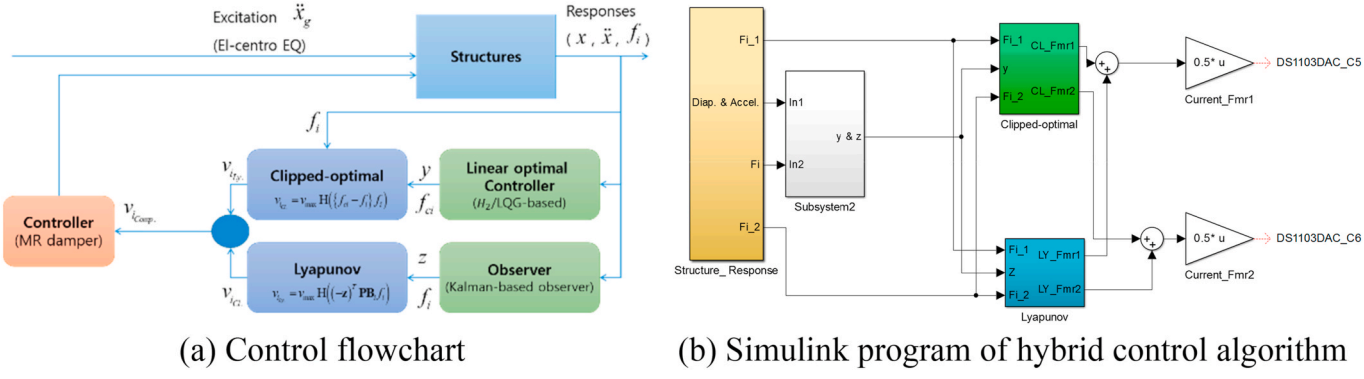

Fig. 6. Hybrid control algorithm.

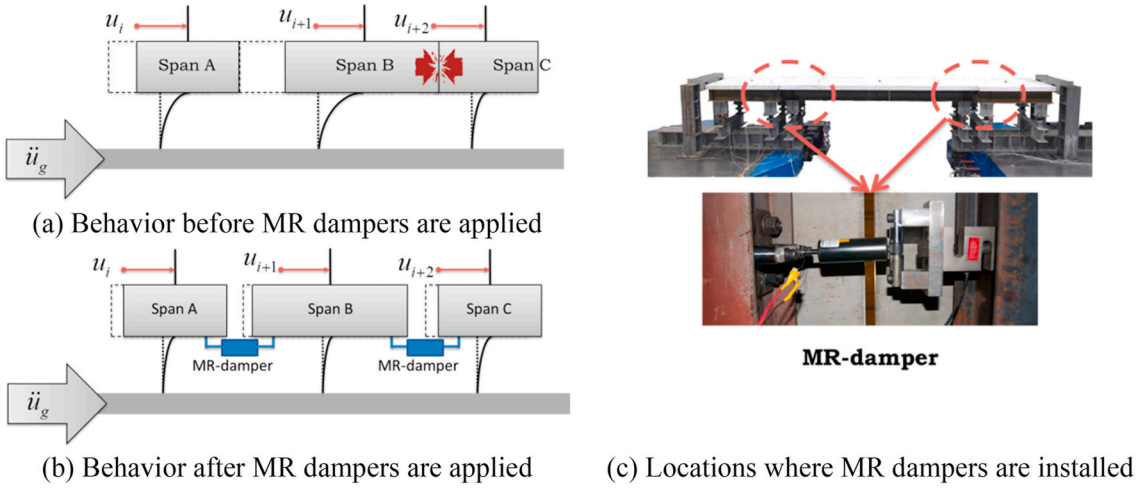

Fig. 7. Multispan isolated bridges.

Table 6
Software for drift control test.

Items	Software
Control Source Coding	Matlab 8.1.0.604 (R2013a)
Control Law Programming	Matlab Simulink
Control GUI Design	Control Desk for dSPACE 1103

running the two shaking tables by using an external force that was equivalent to 40% of the Kobe seismic load (i.e., a load of PGA 0.821 g measured by the KJMA observation center in 1995).

As shown in Fig. 8, there were parts where very small errors occurred in the two shaking tables. However, the error was found to have a slight effect on the test results, and the experiment was continued. The performance evaluation test of the developed hybrid control algorithm was divided into a basic structure state in which no control device was used, a passive state in which a control device was used but no current was supplied, single control states in which the Lyapunov and clipped-optimal control algorithms were individually used, and a state in which the developed hybrid control algorithm was used. As shown in Fig. 8, 40% of the Kobe seismic load was used as the input seismic load, considering the structural damage in the basic structure state when the tests were performed.

Table 7
Hardware for drift control test.

Items		Hardware
Measurement & Control System		dSPACE CP1103
Control Device		RD-8040-1 (MR Damper)
		PMC-18-3A (DC Power Supply)
Sensor	Acceleration	3134D
	Displacement Meter	KTR-B-100 mm
		NSC30-10 (Power Supply)
	Load Cell	DBBP-2t
		DPM-612A (Strain Amplifier)

4.3. Analysis of results from real-time drift control tests

In the real-time drift control tests, the shaking table that held the multispan isolated bridge was moved by a signal that was equivalent to

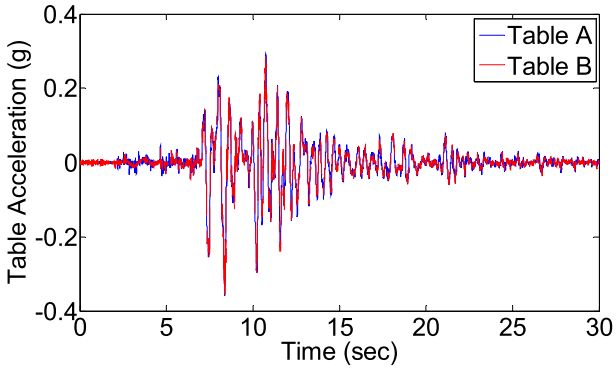

Fig. 8. Synchronization of shaking tables.

40% of the Kobe seismic load, and the measured signals were compared. The graph in Fig. 9 shows a comparison of the acceleration, displacement, and relative displacement response in the basic structure state and the passive state in which the MR damper is used but no current is supplied.

As shown in Fig. 9, Spans A and C of the target bridges showed slightly different movements owing to production and installation errors. Spans A and B as well as spans B and C of the target bridges showed pounding at different times. This amplified the behavior difference between spans A and C. There was no significant difference in responses between the basic structure state and the state in which the adjacent bridge superstructure elements were simply connected by the MR damper. In particular, it was confirmed that the momentary increases in acceleration response that occurred owing to the pounding between adjacent superstructure elements in the basic structure state also occurred in the passive state. Figs. 10 and 11 show graphs in which the basic structure state and the passive state are compared with states in which a current of 2 A was supplied to the MR damper control using the Lyapunov control algorithm and the clipped-optimal control algorithm, respectively.

As shown in Figs. 10 and 11, the results obtained using each of the control algorithms confirmed that there was a reduction in the momentary increase in acceleration response caused by the pounding between adjacent bridge superstructure elements that occurred in the basic structure state and the passive control algorithm state. However, when the Lyapunov control algorithm shown in Fig. 9 was applied, the reduction in pounding between spans A and B was lower than that between spans B and C. Further, when the clipped-optimal control algorithm was applied, the reduction in pounding between spans B and C was lower than that between spans A and B. To determine why these results were obtained, the force–displacement responses of each damper were compared, and the results are shown in Fig. 12.

As shown in Fig. 12, the MR damper that connects spans A and B produces a large control force in the clipped-optimal control algorithm state, and the MR damper that connects spans B and C produces a large control force in the Lyapunov control algorithm state. This behavior of the multispan isolated bridge was determined to occur when the external force acted upon it because a large force was produced in the MR damper that connects spans A and B because the relatively heavy span B supported the drift of span A. The clipped-optimal control algorithm reacted sensitively to this force and produced a large control force because clipped-optimal control mainly plays the role of reducing the external force of the MR damper. In the Lyapunov control algorithm, resistance to the drift of span A occurred because of the support of span B. This was determined to occur because the drift of span C was large, and a large control force was produced to stabilize it because the Lyapunov control algorithm stabilizes the structural system. The graph in Fig. 13 shows the test results for the hybrid algorithm that was developed to compensate for the disadvantages of the individual algorithms.

The graph in Fig. 13(a) shows a comparison of the test results of the hybrid control algorithm with those of the Lyapunov control algorithm and the clipped-optimal control algorithm. As seen in this figure, the hybrid control algorithm achieved satisfactory performance in reducing the pounding response between spans A and B, for which the Lyapunov control algorithm showed inadequate performance, and it achieved satisfactory performance in reducing the pounding response between spans B and C, for which the clipped-optimal control algorithm showed inadequate performance. These results were also confirmed from the force–displacement response graph shown in Fig. 13(b). The hybrid control algorithm achieved similar performance to that of the clipped-optimal control algorithm, which showed excellent performance at spans A and B, and it achieved similar performance to the Lyapunov control algorithm, which showed excellent performance at spans B and C. Tables 8 and 9 show comparisons of the maximum values of the acceleration, displacement, and relative displacement responses to quantitatively confirm the test results.

Tables 8 and 9 show the maximum values of the acceleration and displacement responses according to each test condition and the degree of damping compared with the basic structure state. The rate of reduction in the displacement and acceleration responses was very small in the state in which the dampers were applied to the basic structure but current was not supplied. However, there was a difference in the performance of each control algorithm according to the current supplied to the Lyapunov and clipped-optimal control algorithms. The damping of the acceleration response was confirmed to be ~50% or more in span A, ~30% or more in span B, and ~40% or more in span C. This damping of the acceleration response implies damping of the pounding force between adjacent superstructure elements. Further, the damping of the displacement response was 40% or more in span A, ~20% or more in span B, and ~25% or more in span C. These results imply that the strength of the pounding between adjacent superstructure elements is adjusted by the damping of the drift of the superstructure elements. The relative displacement responses shown in Table 10 have a direct effect on pounding. In the case of the Lyapunov control algorithm, the relative displacement reduction performance of spans B and C was ~10% higher than that of spans A and B. In the case of the clipped-optimal control algorithm, the relative displacement reduction performance in spans A and B was ~5% higher than that of spans B and C. This difference in the relative displacement reductions was determined to be due to the difference between the essential goals of each algorithm. The hybrid

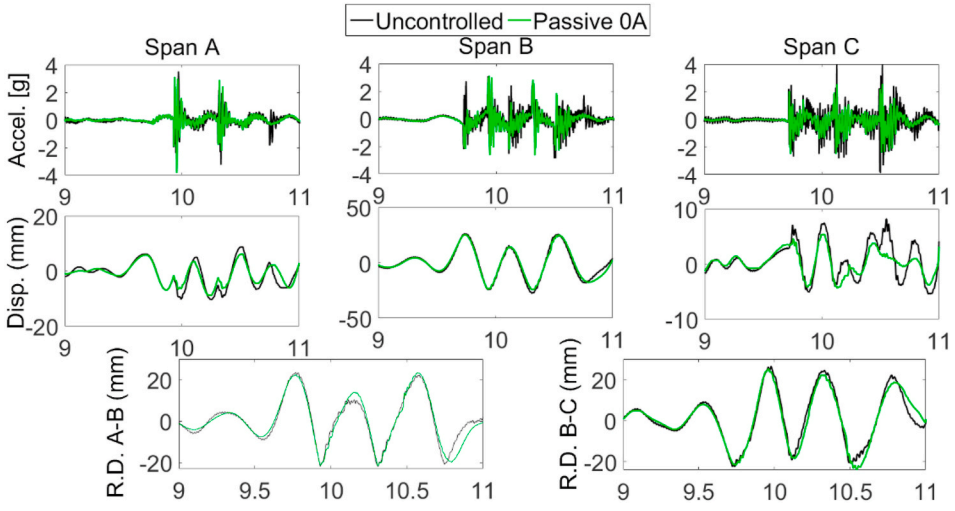

Fig. 9. Drift control test results: uncontrolled vs. passive 0 A.

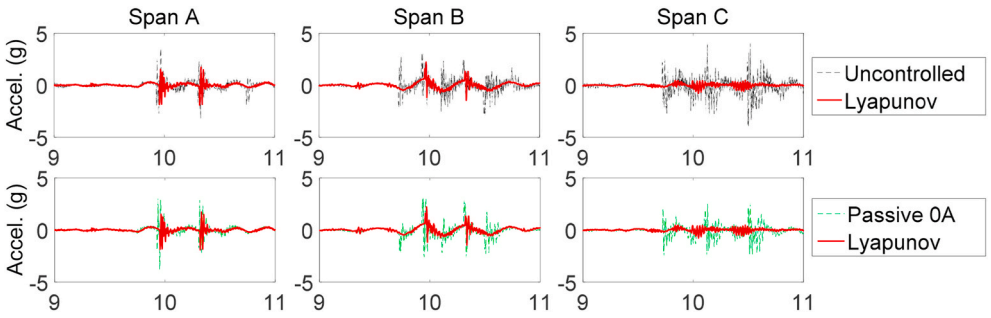

Fig. 10. Drift control test results: uncontrolled vs. Lyapunov control.

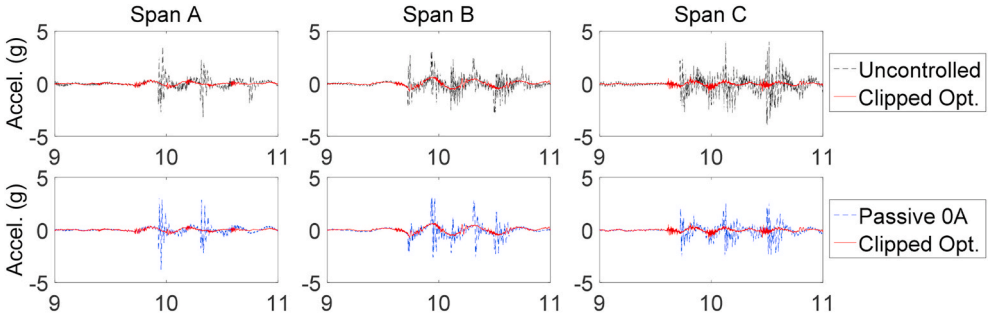

Fig. 11. Drift control test results: uncontrolled vs. clipped-optimal control.

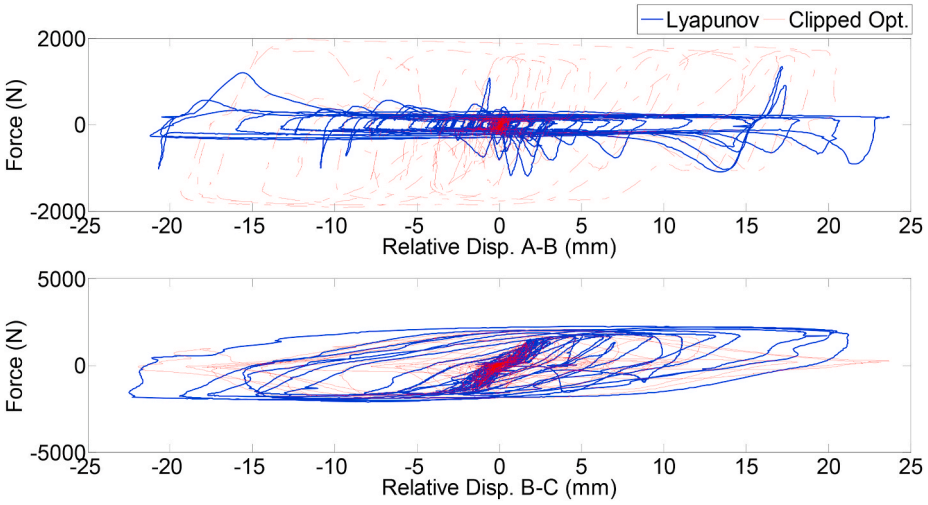

Fig. 12. Force–displacement curve: Lyapunov control vs. clipped-optimal control.

control algorithm was developed to compensate for these differences in each control algorithm, and it showed the best reduction performance with respect to the acceleration and displacement of each superstructure element. As shown in Table 10, the hybrid control algorithm reduced the relative displacement between spans A and B by 50% than in the case when the Lyapunov algorithm alone was adopted. In addition, it reduced the relative displacement between spans B and C by 33% than in the case when the clipped-optimal algorithm alone was adopted. The relative displacement responses are directly related to pounding, and the hybrid control algorithm equally reduced the maximum relative displacement of each connecting section.

5. Conclusion

This study developed a hybrid control algorithm and proved its effectiveness through experiments in which a model bridge was placed on a shaking table to effectively control the drift occurring in the superstructure of an isolated multispan bridge. The following conclusions can be drawn from this study.

1. We calculated the optimal control force for an MR damper to prevent both too much force from causing the spans to work like a unified structure and too little force from causing pounding between spans.

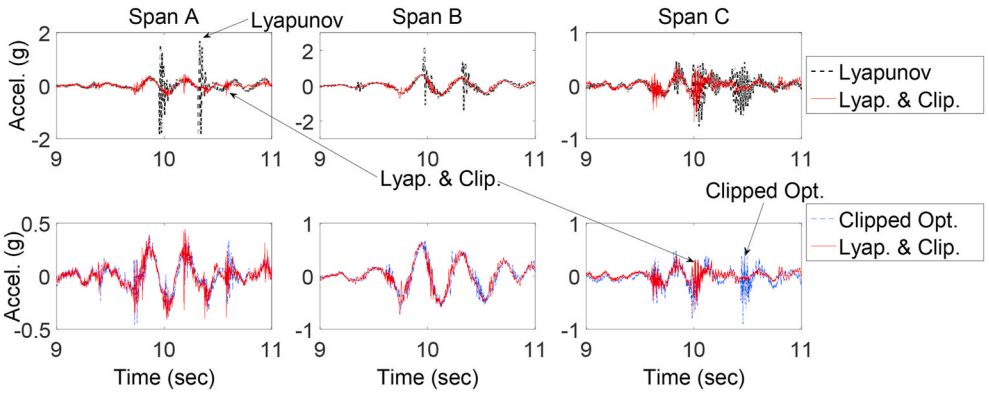

(a) Acceleration response of each span

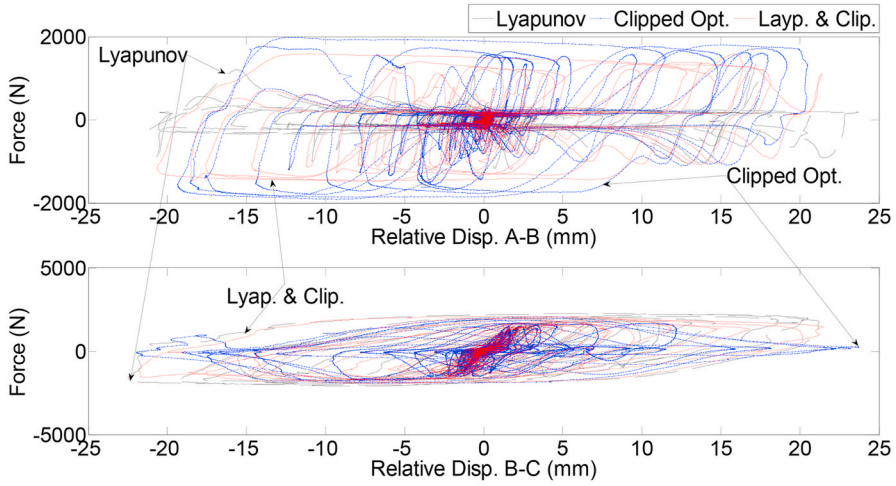

(b) Force–displacement response of MR damper for each control algorithm

Fig. 13. Performance comparison of hybrid control algorithm.

Table 8
Comparison of acceleration.

	Span A		Span B		Span C	
	Max. (g)	Variation of Max. (%)	Max. (g)	Variation of Max. (%)	Max. (g)	Variation of Max. (%)
Uncontrolled	7.5399	–	6.0459	–	7.8979	–
Passive 0 A	6.9580	−7.7	6.0842	+0.63	6.3669	−19.38
Lyapunov	3.6341	−51.80	4.0021	−33.80	3.4705	−56.06
Clipped OPT.	1.1347	−84.95	3.8323	−36.61	4.3536	−44.88
Lyap. & Clip.	0.9216	−87.78	1.3693	−77.35	2.0415	−74.15

Table 9
Comparison of displacement.

	Span A		Span B		Span C	
	Max. (*mm*)	Variation of Max. (%)	Max. (*mm*)	Variation of Max. (%)	Max. (*mm*)	Variation of Max. (%)
Uncontrolled	30.3747	–	62.2123	–	15.5922	–
Passive 0 A	21.0191	−30.80	61.2885	−1.48	14.3133	−8.20
Lyapunov	17.5110	−42.35	50.3017	−19.15	11.5321	−26.04
Clipped OPT.	14.5555	−52.24	48.1933	−22.53	11.7881	−24.40
Lyap. & Clip.	15.5212	−48.90	47.8181	−23.14	10.7538	−31.03

2. We developed a hybrid control algorithm that combined the advantages of the Lyapunov and clipped-optimal algorithms to add a median to the minimum and maximum forces of the MR damper. Through shaking table tests, this algorithm was proved to be effective in reducing the acceleration response by up to 70% as well as in reducing the relative displacement, and it thereby controlled the drift of an isolated multispan bridge.

Therefore, the hybrid control algorithm developed in this study was verified to effectively stabilize the whole structure by controlling the

Table 10
Comparison of relative displacement.

	Relative Dis. A-B		Relative Dis. B–C	
	Max. (*mm*)	Variation of Max. (%)	Max. (*mm*)	Variation of Max. (%)
Uncontrolled	50.411	–	54.287	–
Passive 0 A	49.181	−2.44	53.151	−2.09
Lyapunov	44.942	−10.85	43.721	−19.46
Clipped OPT.	39.829	−20.99	45.657	−15.90
Lyap. & Clip.	42.061	−16.56	43.304	−20.23

drift of the superstructure of multispan bridges.

CRediT authorship contribution statement

G. Heo: Supervision, Methodology, Investigation. **S. Seo:** Formal analysis, Validation. **S. Jeon:** Test, Visualization. **C. Kim:** Conceptualization, Software, Writing - original draft.

Declaration of competing interest

The authors declare that they have no known competing financial interests or personal relationships that could have appeared to influence the work reported in this paper.

Acknowledgments

This research was supported by National Research Foundation of Korea through funding from the Ministry of Education (Project Nos. NRF-2018R1A6A1A03025542 and NRF-2019R1I1A1A01049701). The authors are grateful to the National Research Foundation for making this research possible.

References

[1] Kasai K, Maison BF. Building pounding damage during the 1989 Loma Prieta earthquake. Eng Struct 1997;19(3):195–207.
[2] Lew HS, Coper J, Hacopian S, Hays W. The january 17, 1994, Northridge earthquake, California, vol. 871. National Institute of Standards and Technology; 1994. p. 375–426.
[3] Muthukumar S, DesRoches R. A Hertz contact model with non-linear damping for pounding simulation. Earthq Eng Struct Dynam 2006;35:811–28.
[4] Jeon JS, Seo YD, Choi HS, Park JB. Examples of bridge damage due to earthquakes in Korea. Proc EESK Conf 2018:25–6.
[5] Kawashima K, Matsuzaki H. Damage of road bridges by 2011 Great East Japan (Tohoku) earthquake. Lisboa: 15th World Conference on Earthquake Engineering; 2012.
[6] Domaneschi M, Martinelli L. Earthquake-resilience-based control solutions for the extended benchmark cable-stayed bridge. J Struct Eng 2016;142(8):1–9.
[7] Shehata E, Raheem A. Pounding mitigation and unseating prevention at expansion joints of isolated multi-span bridges. Eng Struct 2009;31:2345–56.
[8] Soong TT, Dargush GF. Passive energy dissipation systems in structural engineering. Wiley; 1997.
[9] Ruangrassamee A, Kawashima K. Experimental study on semi-active control of bridges with use of magnetorheological damper. J Struct Eng 2001;47A:639–50.
[10] Sahasrabudhe SS, Nagarajaiah S. Semi-active control of sliding isolated bridges using MR dampers: an experimental and numerical study. Earthq Eng Struct Dynam 2005;34:965–83.
[11] Nagarajaiah S, Narasimhan S, Agrawal A, Tan P. Benchmark structural control problem for a seismically excited highway bridge—Part III: phase II Sample controller for the fully base-isolated case. Struct Contr Health Monit 2009;16:549–63.
[12] Pourzeynali S, Bahar A. Vertical vibration control of suspension bridges subjected to earthquake by semi-active MR dampers. Sharif Univ Technol 2017;24(2):439–51.
[13] Wang Q, Dong X, Li L, Yang Q, Ou J. Wind-induced vibration control of a constructing bridge tower with MRE variable stiffness tuned mass damper. Smart Mater Struct 2020;29(4).
[14] Bathaei A, Ramezani M, Ghorbani-Tanha AK. Type-1 and Type-2 fuzzy logic control algorithms for semi-active seismic vibration control of the college urban bridge using MR dampers. Civ Eng Infrastruct J 2017;50(2):333–51.
[15] Guo A, Li Z, Li H, Ou J. Experimental and analytical study on pounding reduction of base-isolated highway bridges using MR dampers. Earthq Eng Struct Dynam 2009;38:1307–33.
[16] Sheikh MN, Xiong J, Li WH. Reduction of seismic pounding effects of base-isolated RC highway bridges using MR damper. Struct Eng Mech 2012;41(6):791–803.
[17] Heo G, Kim C, Jeon S, Lee C, Jeon J. A hybrid seismic response control to improve performance of a two-span bridge. Struct Eng Mech 2017;61(5):675–84.
[18] Ali SF, Ramaswamy A. Testing and modeling of MR damper and its application to SDOF systems using integral backstepping technique. J Dyn Syst Meas Contr 2009;131(2).
[19] Achour-Olivier F, Afra H. Lyapunov based control algorithm for seismically excited buildings. Period Polytech Civ Eng 2016;60(3):413–20.
[20] Ali SF, Ramaswamy A. Design optimization of active and passive structural control systems. Info Sci Ref 2013:300–32.
[21] Basili M, De Angelis M. Optimal passive control of adjacent structures interconnected with nonlinear hysteretic devices. J Sound Vib 2007;301:106–25.
[22] El-Khoury O, Kim C, Shafieezadeh A, Hur JE, Heo GH. Experimental study of the semi-active control of a nonlinear two-span bridge using stochastic optimal polynomial control. Smart Mater Struct 2015;24:1–15.
[23] El-Khoury O, Kim C, Shafieezadeh A, Hur JE, Heo GH. Mitigation of the seismic response of multi-span bridges using MR dampers: experimental study of a new SMC-based controller. J Vib Contr 2016;24(1):83–99.
[24] Heo G, Kim C, Jeon S, Lee C, Seo S. A study on a MR damping system with lumped mass for a two-span bridge to diminish its earthquake-induced longitudinal vibration. Soil Dynam Earthq Eng 2017;92:312–29.
[25] Leitmann G. Semi active control for vibration attenuation. J Intell Mater Syst Struct 1994;5:841–6.
[26] Dyke SJ, Spencer Jr BF, Sain MK, Carlson JD. Experimental verification of semiactive structural control strategies using acceleration feedback. Proceeding of the 3rd international conference on motion and vibration control, vol. 3; 1996. p. 291–6.